Journal of
Mechanics of
Materials and Structures

Maria Pilar Ariza and Juan Pedro Mendez

msp

STABILITY OF DISCRETE TOPOLOGICAL DEFECTS IN GRAPHENE

MARIA PILAR ARIZA AND JUAN PEDRO MENDEZ

While improving graphene production techniques seems to be critical for the successful development of practical graphene-based devices, another technological bottleneck stems from the fact that not all mechanisms controlling the coupled thermal-mechanical-electrical behavior of graphene-based materials are fully known at present. In this work, we specifically aim to propose a methodology to investigate the behavior of controlled distributions of point defects in graphene. We present a bondwise force-constant model derived from the adaptive intermolecular reactive empirical bond-order (AIREBO) potential and compare the force-constant values with those obtained from other interatomic potentials. In addition, we present a particular computational scheme that, while preserving the advantages of discrete dislocation theory, allows the assessment of the stability of discrete defects. In particular, we study two dislocation dipole configurations: glide and shuffle.

1. Introduction

Ever since its meteoric rise to prominence, graphene has been touted as a promising novel material, owing to its extraordinary mechanical, electrical, optical and thermal properties. In addition to its high breaking strength and high Young's modulus (42 N/m and 1 TPa [Lee et al. 2008]), graphene exhibits high thermal mobility (> 4000 W/mK [Balandin et al. 2008]), low resistivity ($\approx 30\,\Omega^{-1}$ [Bae et al. 2010]) and high electronic conductivity (> 15000 cm^2/(V · s) [Geim and Novoselov 2007]); i.e., electrons in graphene are allowed to travel long distances without scattering. Other features that have made this material deeply peculiar are its low weight (0.77 mg/m^2), its capability to absorb a fraction of incident white light (around 2.3% [Nair et al. 2008]) and its impermeability to gases [Bunch et al. 2008], among other intriguing properties.

By virtue of these features, today graphene offers a wide range of benefits, and indeed new innovative applications of graphene come to light every day. For instance, graphene has been thought to be an ideal alternative to carbon fibers for structural applications in aeronautics or a substitute of indium tin oxide (ITO) in touchscreens or flexible panel displays [Bae et al. 2010], liquid crystal displays (LCD) [Jung et al. 2014; Blake et al. 2008] and organic light emitting diodes (OLED) [Wu et al. 2010] in optoelectronics. Unfortunately, it was recognized early on [Novoselov et al. 2005; Zhang et al. 2005] that pristine defect-free graphene has no band gap and, therefore, is of limited use for semiconductor-based electronics. Immediately thereafter, many attempts were made to engineer band gaps in graphene, for example by using doped graphene, nanoribbons, electric fields, mechanical strain or engineering defects, among other means [Yazyev and Louie 2010a; Zhang et al. 2012].

Graphene material properties and, in particular, experimentally observed topological defects have been analyzed by using different interatomic potentials and computational approaches ranging from *ab initio* to molecular dynamics. Furthermore, empirical tight-binding models have been applied, allowing for a proper description of the electronic structure of graphene. In particular, Jeong et al. [2008] have studied the stability of dislocation dipoles with 5–7 core structures using *ab initio* calculations whereas Yazyev and Louie [2010b] have focused on the thermodynamics and electronic properties of dislocations and grain boundaries. Molecular dynamics simulations carried out by Liu et al. [2011] investigated the atomic structures and energies of symmetric tilt grain boundaries using the empirical AIREBO potential. The aforementioned potential is an extension of the reactive empirical bond-order REBO potential developed by Brenner [1990], which additionally includes torsion, dispersion and nonbonded repulsion interactions. Thus, the AIREBO potential [Stuart et al. 2000] is suitable for modeling chemical reactions.

We have previously presented [Ariza and Ortiz 2010; Ariza et al. 2010] an analysis of discrete dislocations in graphene based on the discrete dislocation theory in crystals [Ariza and Ortiz 2005]. This said theory combines lattice harmonics, the theory of eigendeformations and the discrete Fourier transform, leading to analytically tractable expressions of the stored energy of defective graphene. In contrast, owing to its reliance on force constants, the theory of discrete dislocations provides harmonic defect structures and their corresponding energies. Therefore, the anharmonic part of the interatomic potentials should be included for the sake of completeness. In this work, we present fully nonlinear solutions obtained by the *method of forces*, i.e., by appending unknown forces to the discrete dislocation energy so as to equilibrate the lattice with respect to the fully nonlinear potential. Specifically, we have first computed the harmonic dislocation core structures and energies predicted by the force constants model obtained from the AIREBO potential and then studied their dynamic stability taking into account the full potential. We have focused on two dislocation dipole configurations: glide and shuffle.

2. The discrete dislocation theory

A general discrete dislocation theory in crystal, and its specialization to graphene, has been presented by Ariza and Ortiz [2005; 2010]. In this section, we present a brief summary of the discrete dislocation (DD) theory extended to graphene. Following this theory, we regard the graphene lattice as a collection of cells $\mathcal{C}$ of different dimensions, endowed with discrete differential operators, discrete codifferential operators and a discrete integral. In particular, the graphene complex is bidimensional and consists of: atoms, or 0-cells; atomic bonds, or 1-cells; and hexagonal cells, or 2-cells (Figure 1). For ease of indexing, we denote by $E_p(\mathcal{C})$ the set of cells of dimension p in the graphene complex and by $e_p(l, \alpha)$ the p-cell of type α and integer coordinates $l \in Z^2$.
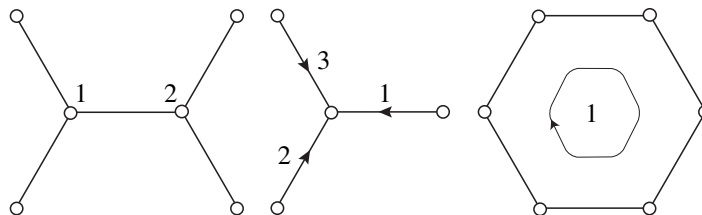
Figure 1. The oriented 0-, 1- and 2-cells of graphene grouped by type.
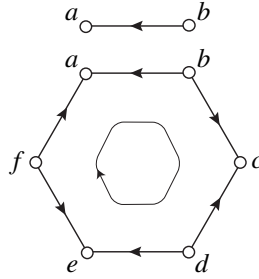
Figure 2. Diagram for the definition of the discrete differential operators of graphene.

These cells provide the support for defining functions, or forms, of different dimensions. Thus, we refer to a function defined over the atoms (or 0-cells), over the atomic bonds (or 1-cells) or over the hexagonal areas (or 2-cells) as a 0-form, 1-form or 2-form, respectively. As we shall see, forms provide the vehicle for describing the behavior of graphene lattice, including displacements, eigendeformations and dislocation densities.

In order to define differential operators, we need to orient all cells; see Figure 2. Suppose that ω is a 0-form defined over the atoms and e_{ab} is an atomic bond defined by atoms a and b and oriented from b to a (Figure 2). Then, the differential $d\omega(e_{ab})$ of ω at e_{ab} is defined as

$$d\omega(e_{ab}) = \omega(e_a) - \omega(e_b). \tag{2-1}$$

Similarly, for 1-forms and 2-forms, we have

$$d\omega(e_{abcdef}) = -\omega(e_{ab}) + \omega(e_{bc}) - \omega(e_{cd}) + \omega(e_{de}) - \omega(e_{ef}) + \omega(e_{fa}) \tag{2-2}$$

and

$$d\omega = \sum_{e_2 \in E_2(\mathscr{C})} \omega(e_2). \tag{2-3}$$

Thus, the differential operator maps: 0-forms, defined over atoms, to 1-forms, defined over atomic bonds; 1-forms, defined over atomic bonds, to 2-forms, defined over hexagonal cells; and 2-forms, defined over hexagonal cells, to vectors. Thus, the defined discrete differential operators may be regarded as the discrete counterparts of the familiar gradient, curl and divergence of vector calculus. It is readily verified from the definition of the discrete differential operators [Munkres 1984] that

$$d^2 = 0, \tag{2-4}$$

which is the discrete counterpart of the identities $\text{rot} \circ \text{grad} = 0$ and $\text{div} \circ \text{rot} = 0$.

Next, by grouping cells of $\mathscr{C}$ by types, one might notice that cells of the same type are translations of each other, and therefore, they are arranged as simple Bravais lattices (Figure 3). Graphene lattice has two different atoms (labeled as 1 and 2), three different atomic bonds (labeled as 1, 2 and 3) and one hexagonal area (labeled as 1). Owing to the translation invariance of the cells, we can take advantage of the definition of the discrete Fourier transform (DFT) and its properties such as the discrete Parseval's identity and the discrete convolution theorem. Thus, the DFT of a p-form ω is

$$\hat{\omega}(\boldsymbol{\theta}, \alpha) = \sum_{\boldsymbol{l} \in \mathbb{Z}^2} \omega(\boldsymbol{l}, \alpha) e^{-i\boldsymbol{\theta} \cdot \boldsymbol{l}}, \tag{2-5}$$
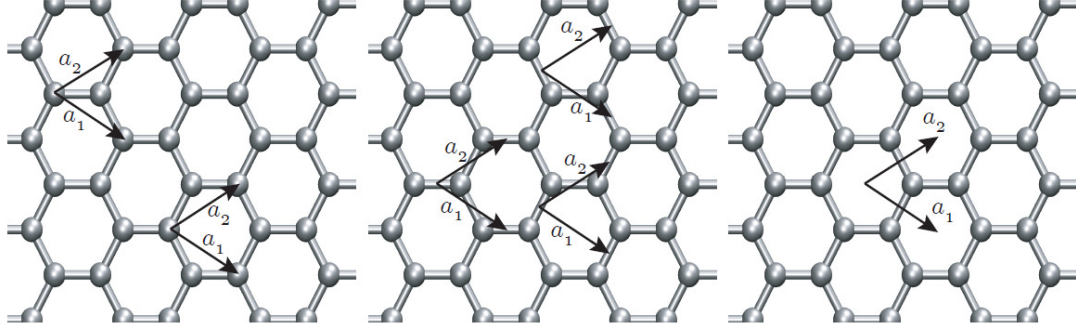
Figure 3. The simple Bravais lattices defined by the atoms, atomic bonds and hexagonal cells of graphene.

where $l \in \mathbb{Z}^2$ are the integer coordinates of the Bravais lattice and α takes the values of 1 or 2 for 0-forms, 1, 2, or 3 for 1-forms and 1 for 2-forms.

Similarly, the DFT of a differential p-form $d\omega$ is

$$\widehat{d\omega}(\boldsymbol{\theta}, \alpha) = \sum_{\beta=1}^{N_p} Q\binom{\boldsymbol{\theta}}{\alpha \ \ \beta} \hat{\omega}(\boldsymbol{\theta}, \beta), \tag{2-6}$$

where the coefficients $Q\binom{\boldsymbol{\theta}}{\alpha \ \ \beta}$ represent the differential structure of the lattice. For the graphene differential structure defined in (2-1) and (2-2),

$$Q_1(\boldsymbol{\theta}) = \begin{pmatrix} 1 & -e^{i\theta_2} \\ 1 & -1 \\ 1 & -e^{-i\theta_3} \end{pmatrix}, \tag{2-7a}$$

$$Q_2(\boldsymbol{\theta}) = (e^{i\theta_3} - 1, 1 - e^{i\theta_1}, e^{i\theta_1} - e^{i\theta_3}), \tag{2-7b}$$

where

$$\theta_3 = \theta_2 - \theta_1. \tag{2-8}$$

Equations (2-7) define the differential of 0- and 1-forms in their Fourier representations, respectively. Within this differential operator framework and by the translational invariance of the energy of lattice, we can write the energy of a harmonic crystal as

$$E(\boldsymbol{u}) = \frac{1}{2} \sum_{e_1 \in E_1} \sum_{e_1' \in E_1} B_{ij}(e_1, e_1') \, du_i(e_1) \, du_j(e_1') \equiv \tfrac{1}{2} \langle \boldsymbol{B} \, d\boldsymbol{u}, d\boldsymbol{u} \rangle, \tag{2-9}$$

where $B_{ij}(e_1, e_1')$ are bondwise force constants, giving the interaction energy resulting from a unit differential displacement in the j-th coordinate direction at bond e_1' and a unit differential displacement in the i-th coordinate direction at bond e_1.

Equivalently,

$$E(\boldsymbol{u}) = \frac{1}{2} \sum_{e_0 \in E_0} \sum_{e_0' \in E_0} A_{ij}(e_0, e_0') u_i(e_0) u_j(e_0') \equiv \tfrac{1}{2} \langle \boldsymbol{A} \, \boldsymbol{u}, \boldsymbol{u} \rangle, \tag{2-10}$$
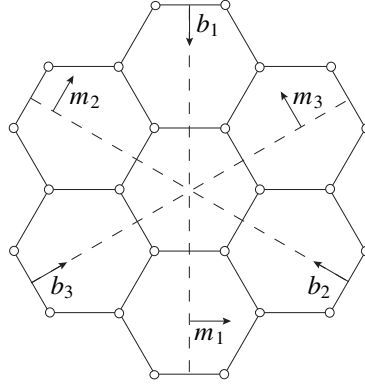
Figure 4. Resulting slip lines and Burger vectors, defining the operative slip systems of graphene.

where $A_{ij}(e_0, e_0')$ are atomic force constants, giving the interaction energy resulting from a unit differential displacement in the j-th coordinate direction at atom e_0' and a unit differential displacement in the i-th coordinate direction at atom e_0.

Moreover, by the translation invariance of lattice, we can express $\boldsymbol{B}\,d\boldsymbol{u}$ and $\boldsymbol{A}\boldsymbol{u}$ in convolution form, and then using the Parseval's identity and the convolution theorem, we express the DFT representation of the harmonic energy as

$$E(\boldsymbol{u}) = \frac{1}{(2\pi)^2} \int_{[-\pi,\pi]^2} \tfrac{1}{2} \langle \widehat{\boldsymbol{\Psi}}(\boldsymbol{\theta})\, \widehat{d\boldsymbol{u}}(\boldsymbol{\theta}), \widehat{d\boldsymbol{u}}^*(\boldsymbol{\theta}) \rangle\, d^2\boldsymbol{\theta}, \tag{2-11a}$$

$$E(\boldsymbol{u}) = \frac{1}{(2\pi)^2} \int_{[-\pi,\pi]^2} \tfrac{1}{2} \langle \widehat{\boldsymbol{\Phi}}(\boldsymbol{\theta})\, \hat{\boldsymbol{u}}(\boldsymbol{\theta}), \hat{\boldsymbol{u}}^*(\boldsymbol{\theta}) \rangle\, d^2\boldsymbol{\theta}. \tag{2-11b}$$

The preceding representations show that the force-constant fields are related by

$$\widehat{\Phi}_{ij} = \boldsymbol{Q}_1^T \widehat{\Psi}_{ij}\, \boldsymbol{Q}_1^*. \tag{2-12}$$

Moreover, it is possible now to achieve an expression for the energy of a defective crystal including dislocations. To accomplish this, we include in (2-9) the eigendeformations $\boldsymbol{\beta}$ corresponding to crystal slips [Mura 1987]

$$E(\boldsymbol{u}, \beta) = \frac{1}{2} \sum_{e_1 \in E_1} \sum_{e_1' \in E_1} \boldsymbol{B}(e_1, e_1')(d\boldsymbol{u}(e_1) - \boldsymbol{\beta}(e_1))(d\boldsymbol{u}(e_1') - \boldsymbol{\beta}(e_1'))$$

$$\equiv \tfrac{1}{2} \langle \boldsymbol{B}(d\boldsymbol{u} - \boldsymbol{\beta}), (d\boldsymbol{u} - \boldsymbol{\beta}) \rangle, \tag{2-13}$$

where the sums take place over the atomic bonds of the crystal lattice, $\boldsymbol{u}(e_0)$ is the atomic displacement of atom e_0, $d\boldsymbol{u}(e_1)$ is the deformation of atomic bond e_1, $\boldsymbol{\beta}(e_1)$ is the eigendeformation at bond e_1 and $\boldsymbol{B}(e_1, e_1')$ are bondwise force constants. The local values $\boldsymbol{\beta}(e_1)$ of the eigendeformation field are constrained to defining lattice-invariant deformations; see Figure 4. And finally, the stored energy of a crystal and the respective displacement field is obtained by minimizing (2-13) with respect to $\boldsymbol{u}$:

$$\inf_{\boldsymbol{u}} E(\boldsymbol{u}, \boldsymbol{\beta}) = E(\boldsymbol{\beta}). \tag{2-14}$$

3. Harmonic graphene model

Bond-order potentials have widely been employed to model complex materials, including C-based materials, e.g., graphite, diamond and graphene. Tersoff potentials [1988] are a clear example of bond-order potentials among others such as Finnis–Sinclair potentials [1984], ReaxFF potential [van Duin et al. 2001] and REBO potentials [Brenner 1990]. The latter one is based on Tersoff potentials with additional terms that correct for an inherent overbinding of radicals and that include nonlocal effects. However, REBO potentials include neither torsion of bonds nor nonbonded interactions; both contributions are crucial to model correctly the behavior of graphene. The AIREBO potential [Stuart et al. 2000], which is derived from the REBO potential, includes these effects through the addition of two new terms: a Lennard-Jones potential, E^{LJ}, accounting for long-range interaction, and a torsion term, E^{tors}.

3.1. *AIREBO potential.* In this section, the AIREBO potential is briefly described and particularized to graphene. This empirical potential consists of a sum of different terms

$$E = \frac{1}{2} \sum_i \sum_{j \neq i} \left[E_{ij}^{\text{REBO}} + E_{ij}^{\text{LJ}} + \sum_{k \neq i, j} \sum_{l \neq i, j, k} E_{kijl}^{\text{tors}} \right], \tag{3-1}$$

where E_{ij}^{REBO} is the REBO interaction, E_{ij}^{LJ} is the Lennard-Jones interaction and E_{kijl}^{tors} is the torsion interaction.

The REBO part combines the repulsive and the attractive terms as

$$E_{ij}^{\text{REBO}} = V_{ij}^R(r_{ij}) + b_{ij} V_{ij}^A(r_{ij}), \tag{3-2}$$

where b_{ij} is the bonding term that specifies the interaction between atoms i and j and their respective neighbors, i.e., b_{ij} depends on the bond angles between the bonding environment surrounding atoms i and j and the bond ij and is a monotonic decreasing function with respect to the coordination number N as $b \sim N^{-1/2}$:

$$b_{ij} = \tfrac{1}{2}[p_{ij}^{\sigma\pi} + p_{ji}^{\sigma\pi}] + \pi_{ij}^{rc} + \pi_{ij}^{dh}. \tag{3-3}$$

The repulsive term exclusively depends on the atom types i and j through the Q_{ij}, A_{ij} and α_{ij} parameters (Table 1) and the bond length r_{ij}:

$$V_{ij}^R = w_{ij}(r_{ij}) \left[1 + \frac{Q_{ij}}{r_{ij}} \right] A_{ij} e^{-\alpha_{ij} r_{ij}}, \tag{3-4}$$

where w_{ij} is a bond weighting factor. Notice that the repulsive term tends to infinity as the bond length between atoms i and j goes to zero.

Parameter	Q_{ij} (Å)	α_{ij} (Å^{-1})	A_{ij} (eV)	$B_{ij}^{(1)}$ (eV)	$B_{ij}^{(2)}$ (eV)	$B_{ij}^{(3)}$ (eV)
CC	0.313460	4.7465391	10953.544	12388.792	17.567065	30.714932
Parameter	$\beta_{ij}^{(1)}$ (Å^{-1})	$\beta_{ij}^{(2)}$ (Å^{-1})	$\beta_{ij}^{(3)}$ (Å^{-1})	ϵ_{ij} (eV)	$\sigma_{ij}^{(2)}$ (Å)	ϵ_{iccj} (eV)
CC	4.7204523	1.4332132	1.3826913	0.00284	3.40	0.3079

Table 1. AIREBO parameters for the attractive, repulsive, LJ and torsion terms.

Parameter	r_{cc} (Å)	N_c	N	s	r'_{cc} (Å)	r^{LJ}_{cc} (Å)	b_{cc}
Minimum	1.7	3.2	2	0.1	1.7	σ_{cc}	0.77
Maximum	2	3.7	3	0.1	2	$2^{1/6}\sigma_{cc}$	0.81

Table 2. Switching parameters between CC bonds.

Similarly, the attractive term also depends on the atom types i and j ($B_{ij}^{(n)}$ and $\beta_{ij}^{(n)}$) and the bond length as

$$V_{ij}^A = -w_{ij} \sum_{n=1}^{3} B_{ij}^{(n)} e^{-\beta_{ij}^{(n)} r_{ij}}. \tag{3-5}$$

The bond weighting factor $w_{ij}(r_{ij})$ smoothly switches off the REBO interaction when the atom pairs exceed the typical bonding distance between carbon atoms for graphene (Table 2):

$$w_{ij}(r_{ij}) = S'(t_c(r_{ij})), \tag{3-6}$$

where $S'(t)$ is

$$S'(t) = \Theta(-t) + \tfrac{1}{2}\Theta(t)\Theta(1-t)[1 + \cos \pi t] \tag{3-7}$$

and $t_c(r_{ij})$ is given by

$$t_c(r_{ij}) = \frac{r_{ij} - r_{ij}^{\min}}{r_{ij}^{\max} - r_{ij}^{\min}}. \tag{3-8}$$

The $p_{ij}^{\sigma\pi}$ and $p_{ji}^{\sigma\pi}$ terms in (3-3) take into account the covalent bond interaction:

$$p_{ij}^{\sigma\pi} = \frac{1}{\sqrt{1 + \sum_{k \neq i,j} w_k(r_k) g_i(\cos\theta_{jik}) + P_{ij}(N_{ij}^C)}}, \tag{3-9}$$

$$p_{ji}^{\sigma\pi} = \frac{1}{\sqrt{1 + \sum_{l \neq i,j} w_l(r_l) g_i(\cos\theta_{ijl}) + P_{ji}(N_{ij}^C)}}, \tag{3-10}$$

$$g_C(\cos\theta_{jik}) = g_C^{(1)}(\cos\theta_{jik}) + S'(t_N(N_{ij}))\big[g_C^{(2)}(\cos\theta_{jik}) - g_C^{(1)}(\cos\theta_{jik})\big], \tag{3-11}$$

where g_i is a penalty function that penalizes the bonds that are very close to one another and θ_{jik} and θ_{ijl} (Figure 5) are the bond angles between the vectors $(\mathbf{r}_i, \mathbf{r}_{ik})$ and $(\mathbf{r}_i, \mathbf{r}_{jl})$, respectively:

$$\cos\theta_{jik} = \frac{\mathbf{r}_i \cdot \mathbf{r}_{ik}}{r_i r_{ik}}, \tag{3-12}$$

$$\cos\theta_{ijl} = \frac{\mathbf{r}_i \cdot \mathbf{r}_{jl}}{r_i r_{jl}}. \tag{3-13}$$

The scaling function $t_N(N_{ij})$ in (3-11) is a function of the local coordination number, N_{ij}, and the upper and lower bound coordination numbers, $N_{ij}^{\max}$ and $N_{ij}^{\min}$, which are related to the material:

$$t_N(N_{ij}) = \frac{N_{ij} - N_{ij}^{\min}}{N_{ij}^{\max} - N_{ij}^{\min}}. \tag{3-14}$$
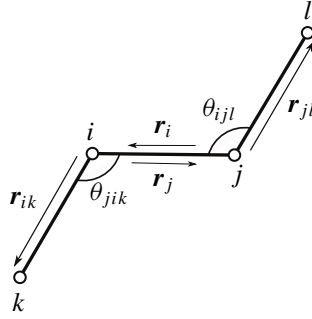
Figure 5. Angle convection.

	$\cos\theta$	g_i	$\partial g_i/\partial\cos\theta$	$\partial^2 g_i/\partial(\cos\theta)^2$
	-1	-0.010000	0.104000	0.000000
	$-\frac{2}{3}$	0.028207	0.131443	0.140229
$g_C^{(1)}$	$-\frac{1}{2}$	0.052804	0.170000	0.370000
	$-\frac{1}{3}$	0.097321	0.400000	1.98000
	1	1.00000	2.83457	10.2647
	-1	-0.010000	0.104000	0.000000
	$-\frac{2}{3}$	0.028207	0.131443	0.140229
$g_C^{(2)}$	$-\frac{1}{2}$	0.052804	0.170000	0.370000
	$-\frac{1}{3}$	0.097321	0.400000	1.98000
	1	8.00000	20.2436	43.9336

Table 3. Interpolation points for the function g_C.

In particular, for graphene,

$$N_{ij} = N_{ij}^C = \left(\sum_{k\neq i}\delta_{kC}w_k(r_k)\right) - \delta_{jC}w_i(r_i). \tag{3-15}$$

The $g_C^{(1)}(\cos\theta_{jik})$ and $g_C^{(2)}(\cos\theta_{jik})$ values and their respective first and second derivatives with respect to the angle in (3-11) are known values and are listed in Table 3.

The third term in (3-3), π_{ij}^{rc}, depends on the coordination numbers. Particularly, π_{ij}^{rc} is zero for graphene lattice with periodic boundary conditions. And the fourth term in (3-3), π_{ij}^{dh}, is based on the torsion angles, w_{kijl}:

$$\pi_{ij}^{dh} = T_{ij}(N_{ij}, N_{ji}, N_{ij}^{\text{conj}}) \sum_{k\neq i,j}\sum_{l\neq i,j}(1-\cos^2\omega_{kijl})$$
$$\times w_{ik}'(r_{ik})w_{jl}'(r_{jl})\Theta(\sin\theta_{jik}-s^{\min})\Theta(\sin\theta_{ijl}-s^{\min}) \tag{3-16}$$

with

$$w_{ij}'(r_{ij}) = S'(t_c'(r_{ij})) \tag{3-17}$$

and

$$t_c'(r_{ij}) = \frac{r_{ij} - r_{ij}^{\min}}{r_{ij}^{\max'} - r_{ij}^{\min}}. \tag{3-18}$$

The torsion angle, w_{kijl}, is defined as the angle between the plane defined by the vectors (r_{ji}, r_{ik}) and (r_{ij}, r_{jl}):

$$\cos \omega_{kijl} = \frac{\boldsymbol{r}_{ji} \wedge \boldsymbol{r}_{ik}}{r_{ji} r_{ik}} \cdot \frac{\boldsymbol{r}_{ij} \wedge \boldsymbol{r}_{jl}}{r_{ij} r_{jl}}. \tag{3-19}$$

The Lennard-Jones term, E_{ij}^{LJ}, in (3-1) includes the long-range interaction between pairs of atoms

$$E_{ij}^{\text{LJ}} = S(t_r(r_{ij}))S(t_b(b_{ij}^*)) + [1 - S(t_r(r_{ij}))]C_{ij}^{\text{LJ}}(r_{ij})V_{ij}^{\text{LJ}}, \tag{3-20}$$

where V_{ij}^{LJ} is a Lennard-Jones potential, 6-12 type,

$$V_{ij}^{\text{LJ}} = 4\epsilon_{ij}\left[\left(\frac{\sigma_{ij}}{r_{ij}}\right)^{12} - \left(\frac{\sigma_{ij}}{r_{ij}}\right)^{6}\right] \tag{3-21}$$

and $S(t)$ is a switching function

$$S(t) = \Theta(-t) + \Theta(t)\Theta(1 - t)[1 - t^2(3 - 2t)]. \tag{3-22}$$

Finally, the torsion term in (3-1), E_{kijl}^{tors}, considers the torsion long-range interaction as a function of the dihedral angle determined by atoms i, j, k and l:

$$E_{ij}^{\text{tors}} = \sum_{k \neq i, j} \sum_{l \neq i, j, k} w_{ij}(r_{ij})w_{jk}(r_{jk})w_{kl}(r_{kl})V_{ijkl}^{\text{tors}}, \tag{3-23}$$

where

$$V_{ijkl}^{\text{tors}} = \epsilon_{ijkl}\left[\frac{256}{405}\cos^{10}\left(\frac{\omega_{ijkl}}{2}\right) - \frac{1}{10}\right]. \tag{3-24}$$

3.2. *Force-constant model.* As proved in Section 2, the energy of a defective crystal lattice can be written in terms of either bondwise force constants, $\boldsymbol{\Psi}$, or atomic force constants, $\boldsymbol{\Phi}$. The former can be obtained through the second linearization of a given interatomic potential; thus, the latter ones are derived by means of relation (2-12). In general, given a potential E, the atomic force constants are obtained by

$$\Psi_{ij}\begin{pmatrix} \boldsymbol{l} - \boldsymbol{l}' \\ ab \quad cd \end{pmatrix} = \frac{\partial^2 E}{\partial r(\boldsymbol{l}', cd)_j \, \partial r(\boldsymbol{l}, ab)_i}, \tag{3-25}$$

where $r(\boldsymbol{l}, ab)_i$ is the i-th component of the vector corresponding to the atomic bond between atoms a and b with label $\boldsymbol{l}$ and $r(\boldsymbol{l}', cd)_j$ is the j-th component of the vector between atoms c and d with label $\boldsymbol{l}'$. Once the bondwise force constants are computed by using the above equation, a straightforward calculation using (2-12) provides the corresponding atomic force constants $\boldsymbol{\Phi}$.

In this section, we tackle the definition of a bondwise force-constants model from the AIREBO potential, and thus, first and second linearizations of energy (3-1) are needed. In order to accomplish an accurate description of interatomic forces in graphene, our model encompasses atomic interactions up to second-nearest neighbors for the REBO term and up to fourth-nearest neighbors for the LJ and torsion terms. The analytical expressions of the first and second derivatives of the functions defining the AIREBO

	(a)	(b)	(c)	(d)	(e)
α_1	364.0	497.2	527.7	409.7	399.0
β_1	247.0	173.8	68.1	145.0	135.7
δ_1	100.5	107.0	118.3	98.9	292.8
α_2	−30.8	−41.4	5.8	−40.8	−79.6
β_2	72.3	58.1	32.7	74.2	67.8
γ_2	−17.8	−3.0	26.7	−9.1	39.2
δ_2	−11.5	−15.9	−16.9	−8.2	0.9
α_3		−20.6	0.0	−33.2	0.0
β_3		34.5	0.0	50.1	0.0
δ_3		9.1	3.7	5.8	−34.3
α_4			0.0	10.5	0.0
β_4			0.0	5.0	0.0
γ_4			0.0	2.2	0.0
δ_4			−1.8	−5.2	17.1

Table 4. Comparison of force-constants values obtained from different interatomic potentials and considering interactions (a) up to second neighbors [Ariza and Ortiz 2010], (b) up to third neighbors [Mendez and Ariza 2015] and (c)–(e) up to fourth neighbors [Ariza et al. 2011; Tewary and Yang 2009; Wirtz and Rubio 2004].

potential have been provided in [Ariza et al. 2011]. Table 4 shows a comparison of the force-constants values we have obtained from the linearization of different interatomic potentials, i.e., a harmonic model [Aizawa et al. 1990], a reactive empirical bond-order potential [Stuart et al. 2000] and a tight binding potential [Xu et al. 1992]. These computed force constants have been validated against experimental phonon dispersion curves and previous force-constants models for graphene. Wirtz and Rubio [2004] have obtained their force constants model by fitting to density-functional theory (generalized-gradient approximation) quantum-mechanics calculations of the phonon dispersion curves of graphene whereas Tewary and Yang [2009] employed a potential based on the Tersoff potential and added a term of radial energy.

4. Anharmonic contribution of the AIREBO potential

The discrete dislocation theory in crystals combines lattice harmonics, the theory of eigendeformations [Mura 1987] and the discrete Fourier transform, leading to analytically tractable expressions of the stored energy of defective graphene (see (2-13)). However, despite its robustness and accuracy, a question of interest concerns the formulation of convergent schemes that relax discrete dislocation structures in accordance to a full interatomic potential. A particular scheme that preserves the advantages of the discrete dislocation theory, and in particular the ability to use Green's functions, was proposed by [Gallego and Ortiz 1993]. In this scheme, the fully nonlinear solution is obtained by the *method of forces*, i.e., by appending unknown forces to the *discrete dislocation* energy so as to equilibrate the lattice with respect to the fully nonlinear atomistic potential.

Thus, given an eigendeformation field, $\boldsymbol{\beta}$, constrained to defining lattice-invariant deformations, the discrete dislocation theory provides a harmonic displacement field, $\boldsymbol{u}_H$, that minimizes the harmonic part

of the potential such that

$$DE_H(\boldsymbol{u}_H) = 0, \tag{4-1}$$

where E_H is the harmonic part of the full potential, $Df(\cdot)$ denotes the derivative of f with respect to its argument and $\boldsymbol{u}_H$ represents the harmonic displacement field corresponding to the eigendeformation field, $\boldsymbol{\beta}$. The total harmonic energy including applied forces $\boldsymbol{f}$ is given by

$$E_H(\boldsymbol{u}, \boldsymbol{\beta}) = \tfrac{1}{2}\langle \boldsymbol{B}(d\boldsymbol{u} - \boldsymbol{\beta}), (d\boldsymbol{u} - \boldsymbol{\beta})\rangle - \langle \boldsymbol{f}, \boldsymbol{u}\rangle = \tfrac{1}{2}\langle \boldsymbol{A}\boldsymbol{u}, \boldsymbol{u}\rangle - \langle \delta(\boldsymbol{B}\boldsymbol{\beta}), \boldsymbol{u}\rangle + \tfrac{1}{2}\langle \boldsymbol{B}\boldsymbol{\beta}, \boldsymbol{\beta}\rangle - \langle \boldsymbol{f}, \boldsymbol{u}\rangle. \tag{4-2}$$

Next, minimization of E_H with respect to $\boldsymbol{u}$ at fixed $\boldsymbol{\beta}$ yields the equilibrium equation

$$\boldsymbol{u}_H^* = \boldsymbol{A}^{-1}(\boldsymbol{f}^E + \boldsymbol{f}), \tag{4-3}$$

where

$$\boldsymbol{f}^E = \delta \boldsymbol{B}\boldsymbol{\beta} \tag{4-4}$$

is the distribution of eigenforces corresponding to $\boldsymbol{\beta}$. We thus continue to apply forces $\boldsymbol{f}$ such that the entire lattice can be equilibrated, and therefore, the resulting harmonic field $\boldsymbol{u}_H^*$ minimizes a given anharmonic energy E. The equilibrium equations for the equilibrating forces $\boldsymbol{f}$ are

$$DE(\boldsymbol{A}^{-1}(\boldsymbol{f}^E + \boldsymbol{f})) = 0. \tag{4-5}$$

Because of the good starting accuracy of the discrete dislocation theory, the corrective forces decay very rapidly away from the core of defects and, hence, represent highly localized corrections.

5. Glide and shuffle dislocation dipoles in graphene

Slip in graphene occurs on three different planes defined by their normal vectors, m_i, $i = 1, 2, 3$, (see Figure 4) which correspond to the close-packed atomic planes in graphene. At first glance, for each slip plane, gliding might occur across either a zigzag chain of bonds or across parallel bonds (Figure 6). The first case defines the so-called glide dislocations whereas the latter one refers to shuffle dislocations.

In a previous work, we have investigated two mechanisms of crystallographic slip in graphene, corresponding to glide and shuffle generalized stacking faults [Ariza et al. 2012]. The calculations were
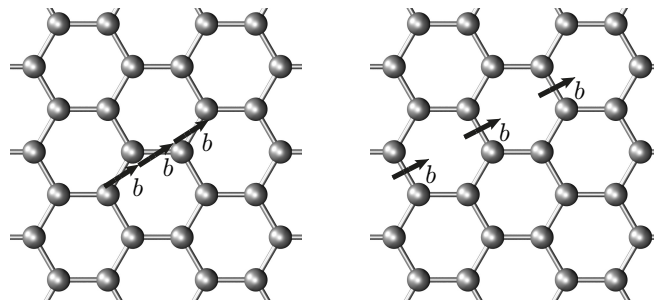
Figure 6. Detail of the distribution of eigendeformation $\boldsymbol{\beta}$, consisting of one Burgers vector over (left) a chain of three zigzag bonds and (right) three consecutive parallel bonds.
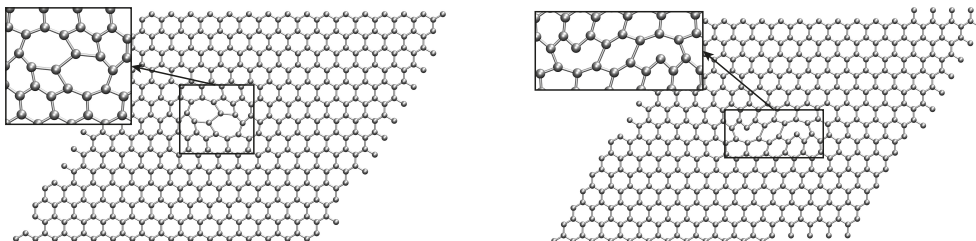
Figure 7. Dislocation core structures predicted by DD theory (left) glide dislocation dipole ($L = 3$) and (right) shuffle dislocation dipole ($L = 3$).
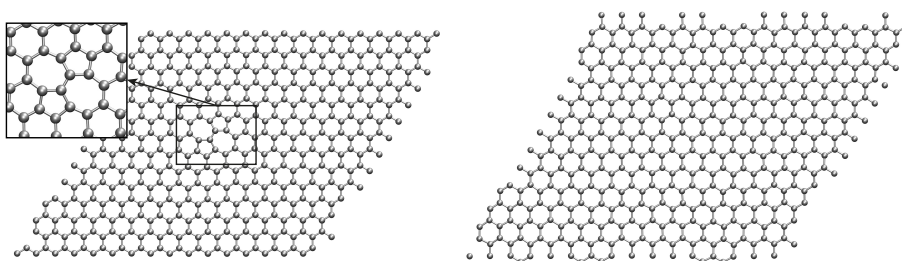
Figure 8. Dislocation core structure after relaxation obtained by means of the anharmonic extension of the DD theory (left) glide dislocation dipole ($L = 3$) and (right) shuffle dislocation dipole ($L = 3$).

performed using the Sandia National Laboratories Large-scale Atomic/Molecular Massively Parallel Simulator (LAMMPS) and two different interatomic reactive potentials: AIREBO and ReaxFF [Stuart et al. 2000; van Duin et al. 2001]. The γ-surfaces of a crystal shed useful light on the structure and stability of extended defects such as dislocation dipoles and dissociated cores. The outcome of the aforementioned study was that glide dislocation dipoles are stable in graphene down to exceedingly small separations of the order of a few lattice spacings and dissociation of perfect dislocations into partial dislocations are unlikely in both configurations. The assessment of the dynamical stability of partial dislocations was carried out by inserting the discrete dislocation configurations predicted by the DD theory into molecular dynamics calculations as initial conditions.

In this section, the stability analysis of discrete dislocation structures is achieved by using the computational scheme outlined above. For ease of indexing, we denote by $L = n$ the length of the dislocation and it represents that the distribution of eigendeformations is applied over n atomic bonds. In this work, we endeavor to assess the stability of glide and shuffle dislocation dipoles. We start by predicting the harmonic core structures and energies of these two dislocations by means of DD theory (see Figure 7). In particular, for configurations corresponding to $L = 3$, we aim to validate our computational scheme by studying whether glide and shuffle dislocation dipoles are metastable or not. Thus, the initial discrete configuration is allowed to relax in accordance to the full interatomic potential AIREBO as was described in Section 4.

Figure 8 shows the computed relaxed configurations and confirms the known metastable character of very short glide dislocations in graphene. Moreover, Table 5 compares the defect energies of the two

Dipole $L = 3$	DD theory (eV)	After relaxation (eV)
Glide	17.07	5.87
Shuffle	20.20	~ 0

Table 5. Computed energies initially predicted by DD theory and obtained after relaxation considering the full interatomic potential for a glide and shuffle dislocation dipole ($L=3$).
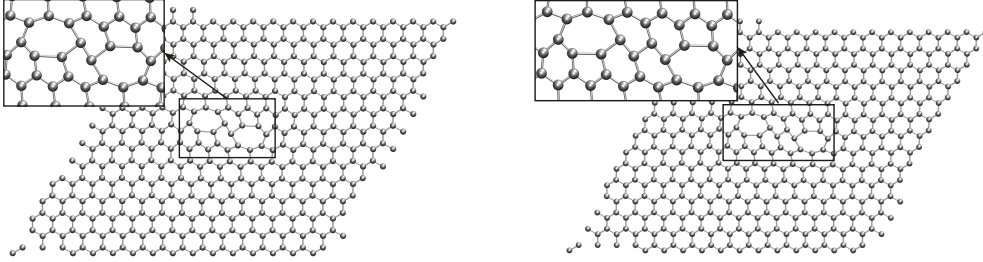
Figure 9. Dislocation core predicted by DD theory (left) glide dislocation dipole ($L = 5$) and (right) glide dislocation dipole ($L = 7$).
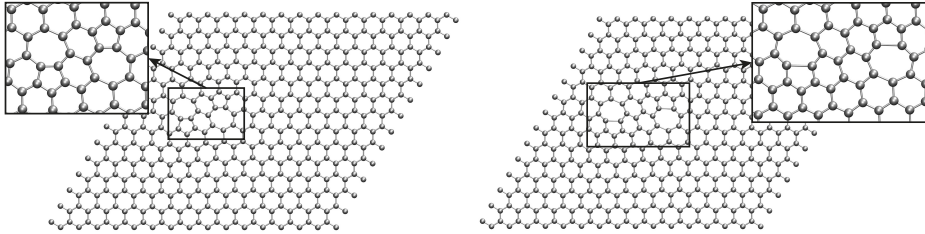
Figure 10. Dislocation core after relaxation (left) glide dislocation dipole ($L = 5$) and (right) glide dislocation dipole ($L = 7$), computed using the extension of the DD theory.

Glide dipole	DD theory (eV)	After relaxation (eV)
$L = 5$	19.87	10.93
$L = 7$	21.74	19.49

Table 6. Stored energies initially predicted by DD theory and those obtained after relaxation considering the full interatomic potential for a glide and shuffle dislocation dipole ($L = 5, 7$).

different dipoles, before and after relaxation. For the shuffle configuration, the stored energy decreases during the relaxation process down to zero.

Next, following the same procedure, we have investigated the relaxed configurations corresponding to two glide dislocation dipoles with $L = 5$ and $L = 7$ (Figures 9 and 10). The stored energies computed before and after relaxation are included in Table 6; these values are in agreement with similar calculations reported in the literature. The relaxed dislocation core structures shown in Figure 10 also agree with those observed in molecular dynamics calculations.

6. Conclusions

We have presented an assessment of the stability of discrete dislocations in graphene. The assessment is based on an extension of the discrete dislocation theory that takes into account the anharmonic part of the interatomic potentials. Thus, we have obtained fully nonlinear solutions by using the *method of forces*, i.e., by appending unknown forces to the discrete dislocation energy so as to equilibrate the lattice with respect to the fully nonlinear potential. Specifically, we have first computed the harmonic dislocation core structures and energies predicted by the force constants model obtained from the AIREBO potential and then studied their dynamic stability.

References

[Aizawa et al. 1990] T. Aizawa, R. Souda, S. Otani, Y. Ishizawa, and C. Oshima, "Bond softening in monolayer graphite formed on transition-metal carbide surfaces", *Phys. Rev. B* **42**:18 (1990), 11469–11478.

[Ariza and Ortiz 2005] M. P. Ariza and M. Ortiz, "Discrete crystal elasticity and discrete dislocations in crystals", *Arch. Ration. Mech. Anal.* **178**:2 (2005), 149–226.

[Ariza and Ortiz 2010] M. P. Ariza and M. Ortiz, "Discrete dislocations in graphene", *J. Mech. Phys. Solids* **58**:5 (2010), 710–734.

[Ariza et al. 2010] M. P. Ariza, M. Ortiz, and R. Serrano, "Long-term dynamic stability of discrete dislocations in graphene at finite temperature", *Int. J. Fracture* **166**:1–2 (2010), 215–223.

[Ariza et al. 2011] M. P. Ariza, C. Ventura, and M. Ortiz, "Modelo de fuerzas interatómicas para el grafeno a partir del potencial AIREBO", *Rev. Int. Métod. Numér.* **27**:2 (2011), 105–116.

[Ariza et al. 2012] M. P. Ariza, R. Serrano, J. P. Mendez, and M. Ortiz, "Stacking faults and partial dislocations in graphene", *Philos. Mag.* **92**:16 (2012), 2004–2021.

[Bae et al. 2010] S. Bae, H. Kim, Y. Lee, X. Xu, J.-S. Park, Y. Zheng, J. Balakrishnan, T. Lei, H. R. Kim, Y. I. Song, Y.-J. Kim, K. S. Kim, B. Özyilmaz, J.-H. Ahn, B. H. Hong, and S. Iijima, "Roll-to-roll production of 30-inch graphene films for transparent electrodes", *Nat. Nanotechnol.* **5**:8 (2010), 574–578.

[Balandin et al. 2008] A. A. Balandin, S. Ghosh, W. Bao, I. Calizo, D. Teweldebrhan, F. Miao, and C. N. Lau, "Superior thermal conductivity of single-layer graphene", *Nano Lett.* **8**:3 (2008), 902–907.

[Blake et al. 2008] P. Blake, P. D. Brimicombe, R. R. Nair, T. J. Booth, D. Jiang, F. Schedin, L. A. Ponomarenko, S. V. Morozov, H. F. Gleeson, E. W. Hill, A. K. Geim, and K. S. Novoselov, "Graphene-based liquid crystal device", *Nano Lett.* **8**:6 (2008), 1704–1708.

[Brenner 1990] D. W. Brenner, "Empirical potential for hydrocarbons for use in simulating the chemical vapor deposition of diamond films", *Phys. Rev. B* **42**:15 (1990), 9458–9471.

[Bunch et al. 2008] J. S. Bunch, S. S. Verbridge, J. S. Alden, A. M. van der Zande, J. M. Parpia, H. G. Craighead, and P. L. McEuen, "Impermeable atomic membranes from graphene sheets", *Nano Lett.* **8**:8 (2008), 2458–2462.

[van Duin et al. 2001] A. C. T. van Duin, S. Dasgupta, F. Lorant, and I. Goddard, W. A., "ReaxFF: a reactive force field for hydrocarbons", *J. Phys. Chem. A* **105**:41 (2001), 9396–9409.

[Finnis and Sinclair 1984] M. W. Finnis and J. E. Sinclair, "A simple empirical *N*-body potential for transition metals", *Philos. Mag. A* **50**:1 (1984), 45–55.

[Gallego and Ortiz 1993] R. Gallego and M. Ortiz, "A harmonic/anharmonic energy partition method for lattice statics computations", *Model. Simul. Mater. Sc.* **1**:4 (1993), 417–436.

[Geim and Novoselov 2007] A. K. Geim and K. S. Novoselov, "The rise of graphene", *Nat. Mater.* **6**:3 (2007), 183–191.

[Jeong et al. 2008] B. W. Jeong, J. Ihm, and G. D. Lee, "Stability of dislocation defect with two pentagon-heptagon pairs in graphene", *Phy. Rev. B* **78**:16 (2008), 165403.

[Jung et al. 2014] Y. U. Jung, K.-W. Park, S.-T. Hur, S.-W. Choi, and S. J. Kang, "High-transmittance liquid-crystal displays using graphene conducting layers", *Liq. Cryst.* **41**:1 (2014), 101–105.

[Lee et al. 2008] C. Lee, X. Wei, J. W. Kysar, and J. Hone, "Measurement of the elastic properties and intrinsic strength of monolayer graphene", *Science* **321**:5887 (2008), 385–388.

[Liu et al. 2011] T.-H. Liu, G. Gajewski, C.-W. Pao, and C. C.-C., "Structure, energy, and structural transformations of graphene grain boundaries from atomistic simulations", *Carbon* **49**:7 (2011), 2306–2317.

[Mendez and Ariza 2015] J. P. Mendez and M. P. Ariza, "Harmonic tight-binding model for graphene", preprint, 2015. To appear in *J. Comput. Phys.*

[Munkres 1984] J. R. Munkres, *Elements of algebraic topology*, Addison-Wesley, Menlo Park, CA, 1984.

[Mura 1987] T. Mura, *Micromechanics of defects in solids*, 2nd ed., Mechanics of Elastic and Inelastic Solids **3**, Kluwer, Dordrecht, Netherlands, 1987.

[Nair et al. 2008] R. R. Nair, P. Blake, A. N. Grigorenko, K. S. Novoselov, T. J. Booth, T. Stauber, N. M. R. Peres, and A. K. Geim, "Fine structure constant defines visual transparency of graphene", *Science* **320**:5881 (2008), 1308.

[Novoselov et al. 2005] K. S. Novoselov, A. K. Geim, S. V. Morozov, D. Jiang, M. I. Katsnelson, I. V. Grigorieva, S. V. Dubonos, and A. A. Firsov, "Two-dimensional gas of massless Dirac fermions in graphene", *Nature* **438**:7065 (2005), 197–200.

[Stuart et al. 2000] S. J. Stuart, A. B. Tutein, and J. A. Harrison, "A reactive potential for hydrocarbons with intermolecular interactions", *Journal of Chemical Physics* **112**:14 (2000), 6472–6486.

[Tersoff 1988] J. Tersoff, "New empirical approach for the structure and energy of covalent systems", *Phys. Rev. B* **37**:12 (1988), 6991–7000.

[Tewary and Yang 2009] V. K. Tewary and B. Yang, "Parametric interatomic potential for graphene", *Phys. Rev. B* **79**:7 (2009), 075442.

[Wirtz and Rubio 2004] L. Wirtz and A. Rubio, "The phonon dispersion of graphite revisited", *Solid State Commun.* **131**:3–4 (2004), 141–152.

[Wu et al. 2010] W. Wu, Z. Liu, L. A. Jauregui, Q. Yu, R. Pillai, H. Cao, J. Bao, Y. P. Chen, and S.-S. Pei, "Wafer-scale synthesis of graphene by chemical vapor deposition and its application in hydrogen sensing", *Sensor. Actuat. B. Chem.* **150**:1 (2010), 296–300.

[Xu et al. 1992] C. H. Xu, C. Z. Wang, C. T. Chan, and K. M. Ho, "A transferable tight-binding potential for carbon", *J. Phys. Condens. Mat.* **4**:28 (1992), 6047–6054.

[Yazyev and Louie 2010a] O. V. Yazyev and S. G. Louie, "Electronic transport in polycrystalline graphene", *Nat. Mater.* **9**:10 (2010), 806–809.

[Yazyev and Louie 2010b] O. V. Yazyev and S. G. Louie, "Topological defects in graphene: dislocations and grain boundaries", *Phy. Rev. B* **81**:19 (2010), 195420.

[Zhang et al. 2005] Y. Zhang, Y.-W. Tan, H. L. Stormer, and P. Kim, "Experimental observation of the quantum Hall effect and Berry's phase in graphene", *Nature* **438**:7065 (2005), 201–204.

[Zhang et al. 2012] J. Zhang, J. Gao, L. Liu, and J. Zhao, "Electronic and transport gaps of graphene opened by grain boundaries", *J. Appl. Phys.* **112**:5 (2012), 053713.

MARIA PILAR ARIZA: mpariza@us.es
Escuela Técnica Superior de Ingeniería, Universidad de Sevilla, Camino de los Descubrimientos, s/n, 41092 Sevilla, Spain

JUAN PEDRO MENDEZ: jmendez@us.es
Escuela Técnica Superior de Ingeniería, Universidad de Sevilla, Camino de los Descubrimientos, s/n, 41092 Sevilla, Spain

msp

JOURNAL OF MECHANICS OF MATERIALS AND STRUCTURES

msp.org/jomms

Founded by Charles R. Steele and Marie-Louise Steele

Special issue
In Memoriam: Huy Duong Bui